Int J Fract (2010) 165:149–162
DOI 10.1007/s10704-010-9458-9

ORIGINAL PAPER

Some aspects of cohesive models and modelling with special application to strength of adhesive layers

Ulf Stigh · K. Svante Alfredsson · Tobias Andersson · Anders Biel · Thomas Carlberger · Kent Salomonsson

Received: 25 September 2009 / Accepted: 1 February 2010 / Published online: 18 February 2010

Abstract An overview of recent development of cohesive modelling is given. Cohesive models are discussed in general and specifically for the modelling of adhesive layers. It is argued that most cohesive models model a material volume and not a surface. Detailed microscopic and mesomechanical studies of the fracture process of an engineering epoxy are discussed. These studies show how plasticity on the mesomechanical length scale contributes to the fracture energy in shear dominated load cases. Methods to measure cohesive laws are presented in a general setting. Conclusions and conjectures based on experimental and mesomechanical studies are presented. The influence of temperature and strain rate on the peak stress and fracture energy of cohesive laws indicates fundamentally different mechanisms responsible for these properties. Experiments and mesomechanical studies show that in-plane straining of an adhesive layer can give large contributions to the registered fracture energy. Finite element formulations including a method to incorporate this influence are discussed.

Keywords Cohesive modelling · Measurement cohesive law · Fracture energy · Traction-separation · J-integral · Adhesive bond

U. Stigh (✉) · K. S. Alfredsson · T. Andersson · A. Biel · T. Carlberger · K. Salomonsson
University of Skövde, Skövde, Sweden
e-mail: ulf.stigh@his.se

1 Introduction

Cohesive models and modelling have seen an almost explosive increase in use and applications during recent years. In the early 60s, Barenblatt (1962) introduced the model to gain insight into the fracture process. In the 70s, Hillerborg et al. (1976) demonstrated the engineering use of the model to predict the strength of structures of concrete. In the 80s applications to strength of composites and adhesive joints were introduced, Bäcklund (1981) and Stigh (1988). In the 80s it was also demonstrated how the model fits within the structure of conventional stress analysis using the finite element method, Needleman (1987) and Stigh (1987). Today, commercial FE-codes incorporate cohesive elements and material laws.

The idea is that crack tips are headed by process zones that can be modelled as cohesive zones. These are surfaces held together by cohesive traction; the traction is assumed to decrease as the surfaces separate. At the end of this process, the traction is zero and new crack surfaces have been created. Figure 1 illustrates a snapshot of a growing crack. The cohesive traction **T** holds the cohesive surfaces together; at the left end, the traction is zero and the cohesive surfaces are transferred into crack faces. At the right end, the cohesive zone is growing into virgin material. As evident, cohesive modelling depicts a process. This can be put into perspective by comparing with classical fracture mechanics. With this model, no process zone is modelled and the crack is assumed to grow when the state at the crack tip is

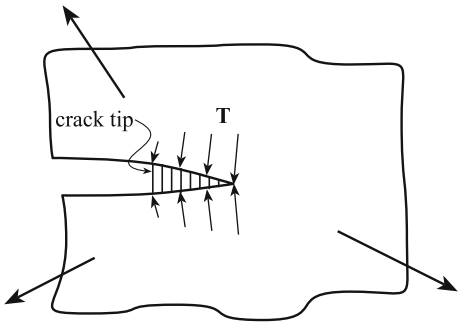

Fig. 1 Cohesive zone heading a crack tip. Traction **T** holds the cohesive surfaces together. In the present paper, the crack tip is considered to be situated at the *left* end of the process zone. It should be noted that the definition of the position of crack tip differs among authors. For instance, in studies of delamination of composites, the *right* end of the process zone is usually considered as the crack tip and the process zone is referred to as a bridging zone

critical. Thus, fracture is not a process but an event. This explains one of the appealing computational features of cohesive modelling as compared to classical fracture mechanics. By modelling a process rather than an event, cohesive modelling fits into the computational scheme of non-linear stress analysis using the finite element method. Compare with the model of fracture mechanics. In linear fracture mechanics, the details of the process zone are ignored based on the notion of an embedded process zone. A stress analysis is first performed on a linearly elastic model without a process zone. The analysis is evaluated to calculate the stress intensity factor K of the crack tip. If K equals the fracture toughness K_c, the state of the crack tip is critical and the crack may grow. The process of growth needs yet another property; usually a criterion of crack growth resistance in terms of an R-curve $K_R(\Delta a)$, where Δa denotes the increase in crack length a. With cohesive modelling, no extra properties are necessary to simulate crack growth. Only the cohesive law is needed to analyze both initiation and growth of a crack. This is also a drawback in modelling flexibility. Namely if the fracture toughness changes with crack growth, a conventional cohesive law cannot capture this phenomenon by itself. Remedies have been suggested in some recent papers, cf. Cox and Yang (2007), Dávila et al. (2009), Yang et al. (2006). In a series of papers, Tvergaard and Hutchinson demonstrate how a conventional cohesive zone model embedded in a volume of plastically deforming material with a remote K-field results in a R-curve behaviour, cf. e.g. Tvergaard and Hutchinson (1992). That is, a carefully performed choice of plasticity and cohesive models may allow for an increasing fracture toughness with crack growth as observed experimentally.

A crack tip within the plastic zone of an ideally plastic material model results in an opening stress of about three times the yield strength σ_Y at the crack tip. This means that a cohesive zone with a peak cohesive stress, $\hat{\sigma}$, larger than about $3\sigma_Y$ will not be activated. That is, $\hat{\sigma}$ must be smaller than about $3\sigma_Y$ for the cohesive zone to make itself noticeable. However, if cohesive zones actually model the separation of atomic layers, $\hat{\sigma}$ ought to be very large, about some fraction of Young's modulus E, cf. e.g. Bao and Suo (1992). Experimentally measured or deduced cohesive laws often show $\hat{\sigma}$ of the same order of magnitude as σ_Y (Andersson and Stigh 2004). That is, orders of magnitude smaller than expected. Moreover, the fracture energy associated with the separation of atomic layers is of the order of 1 J/m^2 which is orders of magnitude smaller than the fracture energy usually associated with cohesive laws.[1] These facts suggest that cohesive models used in most analyzes today, model the behaviour of a material volume. These cohesive laws should therefore be viewed as manifestations of homogenized constitutive properties of material volumes. In turn, this means that the cohesive law is a homogenized property capturing not only separation properties of the material but also elasticity and plasticity. This is apparent of the "fictitious crack model" of Hillerborg. Here, all inelastic material behaviour of the material heading the crack tip is collapsed onto a surface, i.e. the cohesive zone. A fundamental problem with this model is however to identify the volume associated with the cohesive zone. Using the concept of homogenization, the cohesive stress could be expected to result from an analysis of the micromechanics of a representative material volume V_{rep}. That is,

$$\Sigma_{ij} = \frac{1}{V_{rep}} \int_{V_{rep}} \sigma_{ij} \mathrm{d}V \tag{1}$$

where σ_{ij} is the local stress due to a deformation state enforced on the outer surface of V_{rep} corresponding to a

[1] It may be noted that some experiments with extremely thin adhesive layers show interesting properties, cf. e.g. Chai (1986). However, the fracture energy is still very different from what is expected from atomistic analyses.

nominally uniform state of strain E_{ij} of a homogeneous material volume. The idea is that the relation between Σ_{ij} and E_{ij} can replace the detailed properties of the inhomogeneous material in studies of material behaviour on length scales larger than V_{rep}. In such studies, the material can be considered as homogeneous and represented by the homogenized material behaviour. Implicit in the concept is that V_{rep} is large enough. To decide how large is large enough, one may imagine a process where the volume surrounding a material point is allowed to gradually increase until the relation between Σ_{ij} and E_{ij} is virtually unaffected by further increasing the size.

Now, this concept is troublesome when local separation and softening is allowed on the smaller length scale. A fracture process is normally associated with a localization to one dominating defect and a softening of the material at the defect. This process introduces a possibility for instability, where the elastic energy of the material outside the dominating defect rushes to the defect leading to an uncontrolled growth of the defect. A larger volume corresponds to more elastic energy and a decreased likelihood to capture a softening cohesive law. Thus, the concept of choosing larger and larger V_{rep} as discussed above will not likely yield useful results. This problem should not be considered as a mere mathematical feature of the formal mathematical procedure of homogenization. If uncontrolled growth of one dominating defect can be inhibited and a large number of defects are activated in the fracture process, a larger fracture energy will result. An example is provided by the development of rubber modified adhesives, cf. e.g. Kinloch (1987). Here small rubber particles are dispersed into an epoxy matrix. If the rubber particles adhere well to the matrix, they can be elongated to a large extent during the fracture process and hinder uncontrolled growth of itself. By this, more rubber particles are activated and the fracture energy increases. On a structural length scale, a similar process leads to improved fracture energy for adhesives. By constraining the adhesive layer with stiff adherends[2], the fracture process zone gets large; the softening zones at the most deformed part are limited in their growth by the inability of the material to deform due to the constraints of the adherends. This leads to the activation of a large number of softening zones and a larger fracture energy. It also leads to a dramatically larger fracture strain than expected from ordinary tensile tests. In a tensile test, epoxies fracture at a strain of the order of 1%; in the constrained state of an adhesive layer, the engineering strain at fracture is of the order of 100% (Andersson and Stigh 2004).

In this paper, we will discuss cohesive laws of adhesive layers. In this case, the volume represented by the cohesive law is easier to identify. It is determined by the thickness of the adhesive layer. The length and width can be decided using a similar method as discussed above, i.e. letting them increase in size until the homogenized cohesive law is virtually unaffected by the size (Salomonsson and Andersson 2008). It is noted that cohesive laws for adhesive layers have been denoted "traction-separation laws" and "stress-elongation relations" in the literature. The fracture process of a representative engineering epoxy adhesive is first described in some detail. Results from an in-situ SEM study and microscopic studies of the fracture process will be given. Methods to measure cohesive laws are presented in a systematic manner in the following section. This section is followed by a presentation of mesomechanical studies of the same adhesive. In Sect. 5, aspects of cohesive modelling on the structural length scale are discussed and some computational aspects are given. The paper ends with a section with the major conclusions.

2 Fracture processes of adhesive layers

Engineering adhesives are complex materials designed to fulfil a number of requirements such as wetting the bonded parts in its unhardened state. The present adhesive, DOW Betamate XW 1044-3, is a one-component heat-hardening epoxy based adhesive used in the body shop by the car industry. It appears to be generic for many epoxy adhesives used in industry. Figure 2 shows a SEM image of the hardened and unloaded adhesive with a layer thickness of about 0.2 mm. The dark continuous phase in the adhesive is identified as a blend of epoxy and a thermoplastic. In this epoxy, light needle shaped mineral particles form clusters that are randomly oriented in the epoxy matrix. Apart from filling the epoxy with a relatively inexpensive material, the mineral plays an important part in the fracture process.

When loading the adhesive in peel, i.e. by separating the adherends vertically to elongate the adhesive layer, the metallic adherends constrain the adhesive layer so

[2] Adhesively bonded parts are often referred to as adherends.

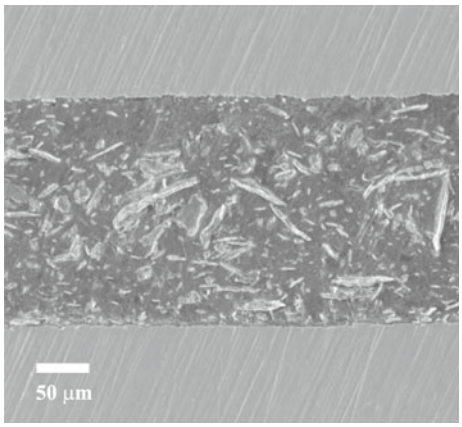

Fig. 2 Layer of hardened engineering epoxy. Dark matrix consists of epoxy blended with a thermoplastic. Light needle shaped particles consist of clusters of mineral pins

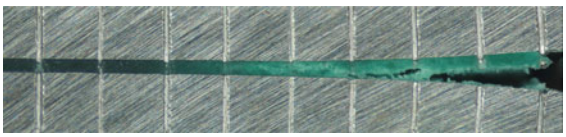

Fig. 3 Damage process of an adhesive. Crack tip to the right; to the left undamaged adhesive with a nominal thickness 0.2 mm. Specimen marked with vertical scratch marks every millimeter

that virtually no macroscopic straining occurs in the in-plane direction. At the start of the adhesive layer, the constraint is less severe, and in-plane straining occurs to allow for the stress free boundary. However, only a few layer thicknesses into the adhesive layer, the constraint has built-up and the condition of zero in-plane strain is fulfilled (Carlberger et al. 2008). The condition of zero in-plane straining was assumed in the seminal paper by Goland and Reissner (1944) and has been given a theoretical footing in asymptotic analyses (Schmidt 2008). Moreover, as seen in Fig. 3, the size of the process zone heading a crack-tip in an adhesive layer is very long. This gives some support to ignore the fine details of the stress field at the crack-tip. However, attempts have been made to track the strength of adhesive joints to the singular elastic field at the corner of the adhesive and adherend (Groth 1988), or to more detailed stress analyses of the state at the free end of an adhesive layer (Adams et al. 1997). If these singularities and details would be decisive for the strength of an adhesive joint, the technological importance of adhesive joining would be very small indeed. It would imply that adhesive joining should be performed with exceedingly

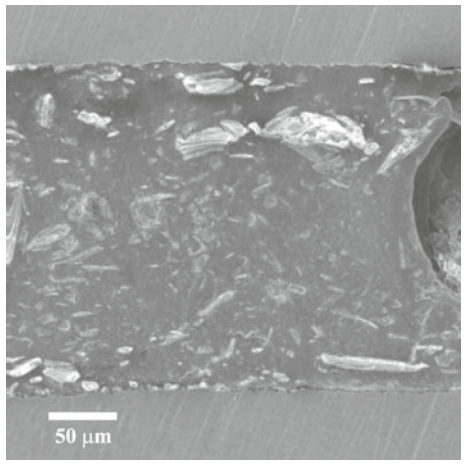

Fig. 4 Adhesive layer after some peel loading

high precision. The experience differs, adhesive joining can be done on an industrial scale leading to adequate quality. It is however plausible that the finer details of the stress field is more important to understand other properties such as fatigue. In this case, the loading is lower and the size of the damage zone is smaller. Especially, in the technologically important case of high cycle fatigue, the detailed stress field might be more important since the loading is low. However, for prediction of strength, today the assumption of zero in-plane straining appears to be almost generally accepted.

Figure 4 shows a SEM image of the same adhesive layer as in Fig. 2 after some peel loading. The present image is taken somewhat closer to the loaded free edge of the adhesive layer; the free edge is seen at the right end of the image. Stress whitening occurs at the mineral particles. Here, it can be deduced that large local vertical strains accumulate. It is also observed that, at this stage, stress whitening occurs at many mineral particles above and below each other. That is, stress whitening at one particle does not lead to total unloading by stress shadowing of particles below or above a softening particle. This observation gives a clue to the reason for the experimentally observed increase in fracture energy with layer thickness (Carlberger 2008). With extremely small layer thicknesses, a limited number of energy consuming particles might be present in the volume heading a crack. With gradually increasing layer thickness, more particles will be available per unit crack area; first in the vertical direction and then in the horizontal direction. The particles consume energy during the fracture process resulting in larger

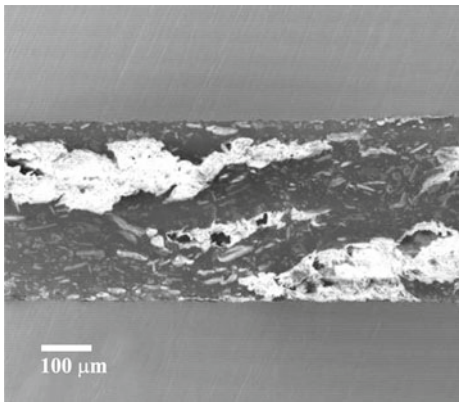

Fig. 5 Adhesive layer close to fracture

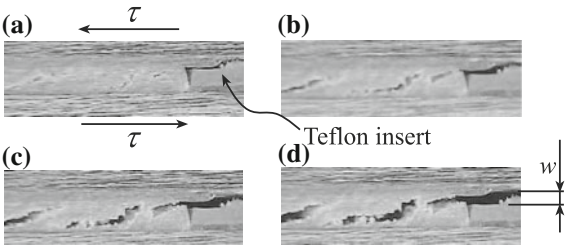

Fig. 6 Deformation process of the adhesive layer during a shear experiment. Images (**a**), (**b**) (**c**) and (**d**) are in consecutive order. The Teflon insert at the *right* end in each image is 0.2 mm thick. The adhesive layer is observed at the free surface of the specimen. Due to a minute grading of the adherends, the layer appears thicker than the teflon insert. The peel separation w in image (**d**) is substantial, Leffler et al. (2007)

fracture energy with a thicker layer. At some critical thickness, the vertical distance between the particles is so large that further increase of layer thickness provides no more increase in fracture energy.

In Fig. 5, the adhesive is in a later state of loading. Some of the volumes of stress whitening have now coalesced. Some voids also appear in the stress whitening areas and we can start to imagine how a final crack will develop from right to left in the image. Still at this stage, voids and stress whitening are active on different layers in the vertical direction.

In shear, the fracture process shows some similarities and differences to the process in peel. Figure 6 shows the fracture process of the same adhesive loaded in shear; images a, b, c and d are taken in consecutive order (Leffler et al. 2007). The first signs of microscopic cracks are observed some distance from the crack tip. A little later in the process, a number of slanted microscopic cracks are visible. At the same

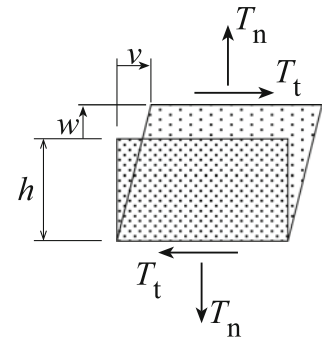

Fig. 7 Conjugated stress and deformation measures on a structural length scale

time, the adherends are observed to move vertically apart, cf. Fig. 6. Thus, the adhesive layer is deformed in mixed mode although the layer is loaded in almost pure shear. It is often assumed that the microscopic cracks should open in 45° to the horizontal direction, so that the cracks open in the direction of the principal tensile stress. Remembering that shear deformation is isochoric, it is understood that the adhesive layer must deform in peel to allow the cracks to grow to voids. This observation leads to a question of the definition of pure shear loading. One may consider two possibilities: with shear deformation v, either peel deformation w or peel stress T_n should be zero, cf. Fig. 7. It is hard to imagine that any of these conditions can be achieved experimentally. As expected, numerical simulations shows that $w = 0$ leads to a much larger fracture energy than the condition $T_n = 0$ (Salomonsson 2008).

As deduced from these images, the local fields within an adhesive layer are extremely complex. In Sect. 4, attempts to model the details of the fracture process are presented. As shown, this leads to an increased understanding of the process. However, if simulations in the design process of adhesively bonded structures would depend on the success of such detailed stress analyses, it would be practically impossible to use adhesives in modern product development. Fortunately, cohesive modelling has proven accurate enough in many situations, cf. Sect. 5. In this model, the adhesive layer is assumed to deform in a combination of peel, w, and shear, v, with conjugated stresses, T_n and T_t, cf. Fig. 7. In 3D, the shear components v and T_t are both split in two orthogonal components.

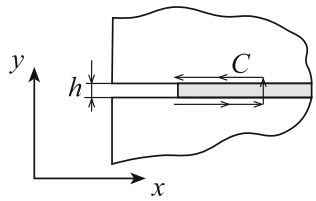

Fig. 8 Internal integration path

3 Experimental measurement of cohesive laws

A number of techniques have been developed to deduce or measure cohesive laws. The methods of deducing cohesive laws are based on experimental observations and fitting simulation models to the results. By systematically adjusting the properties of the simulation model until a good fit is achieved, the main properties of the cohesive law are expected to be deduced (Yang and Thouless 2001). These methods are critically dependent on the sensitivity of the measured properties to the details of the cohesive law. It has however been observed that many of the experimental set-ups used with these methods are insensitive to the details of the cohesive law. A recent and systematic attempt to overcome this problem is presented in Sun et al. (2008). Here a number of fundamentally different experimental set-ups are used synergetically; some of the methods are sensitive to one property of the cohesive law and some to another. By use of many different methods, the main properties of the cohesive law are deduced.

A fundamentally different path is taken in a series of papers, cf. e.g. Andersson and Stigh (2004), Sørensen and Jacobsen (1998). Here, the cohesive law is measured directly. The fundamental assumption in these methods is that a unique cohesive law exists. If this is the case, and if a test specimen is cleverly designed, the path independence of the J-integral can be utilized to derive useful relations between the external loads acting on the specimen and the cohesive law. The J-integral is given by

$$J = \int_{\mathcal{C}} \left(W \, \mathrm{d}y - T_i u_{i,x} \, \mathrm{d}\mathcal{C} \right). \tag{2}$$

where C is any counterclockwise integration path, starting at the lower end of the crack-tip and ending at the upper end, cf. Fig. 8 and Rice (1968). In Eq. (2), T_i and u_i are the i-components of the traction and displacement vectors, respectively; summation is indicated by repeated indexes. Formally, the strain energy density W must exist. However, if no unloading occurs during an experiment from a plastically deformed state and with a stationary crack, the fields are not very different from those obtained if the material behaved according to a deformation type theory. In this case, a pseudo potential can often be defined (Nilsson 2001). Considering the complex loading of an adhesive layer on a micromechanical length scale as depicted in Figs. 4, 5 and 6, it can be concluded that a deformation type theory would be incapable of reproducing these fields. However, on the structural length scale, where the adhesive layer is represented by a cohesive zone, the details of the local fields are represented by the properties of the cohesive law and a pseudo potential can be defined on this length scale. In Andersson and Stigh (2004), the condition is carefully checked on the structural length scale and it is concluded that experiments can be performed that allow for the use of a pseudo potential. Moreover, the pseudo potential is not allowed to be explicitly dependent of the x-coordinate for J to be path independent. This condition is equivalent of assuming the existence of a unique cohesive law.

By evaluating J using the internal integration path shown in Fig. 8, one gets

$$J = \int_0^w T_\mathrm{n} \mathrm{d}\hat{w} + \int_0^v T_\mathrm{t} \mathrm{d}\hat{v} \tag{3}$$

That is, J equals the sum of the areas below the T_n vs. w- and T_t vs. v-curves during an experiment. Note that by measuring J continuously during an experiment and differentiating J with respect to w and v, the cohesive laws T_n vs. w and T_t vs. v are derived. It is likely that these laws are dependent of the particular deformation path, i.e. the relation w/v during the experiment.

By using prismatic, beam-like, test specimens, an external integration path gives a useful complement to Eq. (3). Studying the terms in Eq. (2) reveals that no traction free surfaces contribute to the second term in the integrand. Moreover, no horizontal paths contribute to the first term. That is, contributions will only appear from applied loads and vertical paths where the material is stressed, i.e. where $W \neq 0$. A number of such specimens have been developed during recent years to measure cohesive laws. To be systematic, we may consider three typical loads acting on a beam with the width B and height H: a transversal force, P, a normal force, N, and a bending moment, M, cf. Fig. 9.

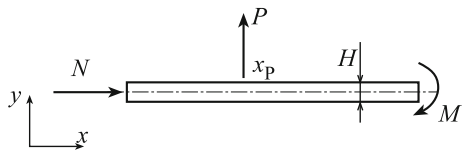

Fig. 9 Three typical loads acting on a beam

Evaluation of Eq. (2) assuming the fields of linear elastic Euler-Bernoulli beam theory to be adequate, gives

$$J = \frac{P\theta}{B} + \frac{6M^2}{EB^2H^3} + \frac{2N^2}{EB^2H} \tag{4}$$

where θ is the rotation of the loading point, and E Young's modulus, cf. Olsson and Stigh (1989), Paris and Paris (1988), Alfredsson (2003), Högberg et al. (2007). It should be noted that by replacing θ with $\sin\theta$, the first term is given its proper large deformation form, cf. Nilsson (2006). Moreover, this term does not rest on the assumption of Euler-Bernoulli beam theory. In the evaluation of Eq. (2) for P, the second term contributes. With $\mathrm{d}\mathcal{C} = -\mathrm{d}x$, $T_x = 0$, and $T_y = P\delta(x - x_P)/B$ direct evaluation yields the first term in Eq. (4)[3]. By combining the relevant terms from Eq. (4) for a specific test specimen, the alternative expression for J is derived. The procedure of an experiment is to measure the history of M, P, N, and θ which yields the evolution of J during the experiment. By measuring corresponding values of v and w at the crack tip, differentiation yields the cohesive law for the particular experiment.

Figure 10 shows a number of specimens developed and used to measure cohesive laws. The Double Cantilever Beam specimen loaded with transversal forces (DCB) and bending moments (DCB-M) are developed and used in a series of papers (Andersson and Stigh 2004; Carlberger et al. 2008; Sørensen and Jacobsen 1998; Alfredsson 2003; Högberg et al. 2007; Andersson and Biel 2006; Carlberger et al. 2009; Alfredsson 2004). Both specimens measure the cohesive law in pure peel loading, i.e. Mode I of fracture mechanics. Both methods necessitate the development of some special features of the test set-up; with the DCB specimen, the rotation of the loading point should be measured and with the DCB-M specimen, the specimen is loaded with bending moments. The End Notched Flexure (ENF) specimen is developed to measure cohesive laws in

[3] It is still necessary to be able to define a pseudo potential for the material in order for J to be path independent.

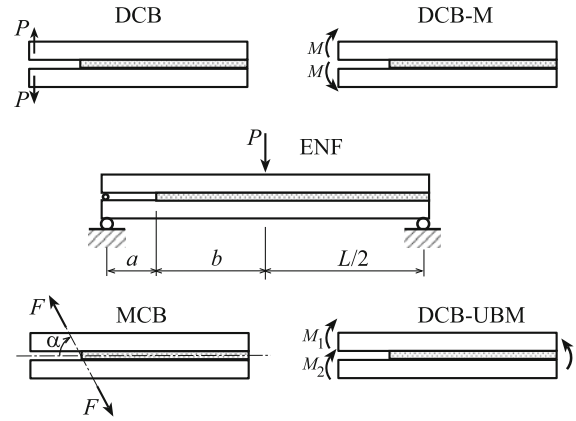

Fig. 10 Specimens developed and used to measure cohesive laws

almost pure shear, cf. Leffler et al. (2007), Alfredsson (2004), Stigh et al. (2009). With the Mixed Mode DCB specimen (MCB) and the DCB specimen loaded by uneven bending moments, methods are developed that allows to measure cohesive laws in mixed mode, cf. Högberg et al. (2007), Sørensen and Kirkegaard (2006). Table 1 summarizes the expressions for J derived for these specimens. In the table, $\theta_1, \theta_2, \theta_3$ for the ENF-specimen, are the clockwise rotations of the three loading points, from left to right, (Stigh et al. 2009); for the MCB-specimen θ_1, θ_2 denote the clockwise rotations of the upper and lower loading points, respectively.

Experimental techniques have been developed for the use of these methods. In general, an experiment is conducted by applying the acting loads by prescribed displacements of the loading points. The relevant loads, rotations, elongation, w, and shear, v, of the adhesive layer are measured continuously during the experiment. From the loads, the evolution of J is calculated using the relevant equation from Table 1. Using the path independence of J and Eq. (3), the evolution of J is connected to the cohesive law. Differentiation of J with respect of w and v yields T_n and T_t, respectively. Differentiation is simplified by first using a least square adaption of J to a reasonable series of functions, cf. e.g. Högberg et al. (2007), Andersson and Biel (2006).

Often, specimens used to measure properties of thin layers are prone to instability. If the loading is applied as prescribed forces or bending moments, most specimens are unstable in the sense that a small increase in crack length leads to an increase in J. If the crack grows under constant fracture energy, the crack will then grow

Table 1 Expressions for J derived for the specimens in Fig. 10

Specimen	J	Reference
DCB	$2P\theta/B$	Olsson and Stigh (1989), Paris and Paris (1988)
DCB-M	$12M^2/EB^2H^3$	Rice (1968)
ENF	$P(\theta_1 - 2\theta_2 + \theta_3)/2B$	Stigh et al. (2009)
MCB	$F\sin\alpha(\theta_1 - \theta_2)/B + 4(F\cos\alpha)^2/EB^2H$	Högberg et al. (2007)
DCB-UBM	$\left[21(M_1^2 + M_2^2) - 6M_1M_2\right]/4EB^2H^3$, where $\lvert M_1\rvert < M_2$	Sørensen and Kirkegaard (2006)

dynamically. By using this criterium for instability, it is shown in Alfredsson and Stigh (2009) that transversely loaded slender specimens loaded by prescribed *displacements* are stable if the crack length is larger than a_{cr} given by

$$\frac{a_{\mathrm{cr}}}{L} = \sqrt[3]{\frac{3c_0}{4\bar{J}}} \tag{5}$$

where

$$c_0 = \frac{EBH^3}{L^3}C(0) \tag{6}$$

is a non-dimensional form of the flexibility of the specimen. Here Δ denotes the load point displacement, $C(0)$ is defined as $C(a) = \Delta/P$ for zero crack length ($a = 0$). This property of the specimen is often easy to calculate; L is the length of the specimen and $\bar{J} = EB^2H^3J/P^2a^2$ is a non-dimensional form of J. This criterium is based on the assumption that Euler-Bernoulli beam theory is accurate enough to capture the flexibility of the specimen and that the effects of the thin layer on the flexibility can be neglected. In Alfredsson and Stigh (2009) it is shown that the effect of transverse shear flexibility of the beams is to promote instability and a flexible interphase layer promotes stability.

Experiments conducted to reveal possible influences of the properties of the adherends, e.g. thickness and material have not revealed any significant influences on cohesive laws (Leffler et al. 2007; Andersson and Biel 2006). This supports the usefulness of cohesive models. However, the thickness of the adhesive layer influences the cohesive law significantly, cf. Carlberger (2008). This is expected since it has long been recognized that the fracture energy depends on the thickness of adhesive layers, cf. e.g. Kinloch (1987). Experiments show that the total area under the cohesive law, i.e. the fracture energy, depends on the layer thickness. However, the peak stress of the cohesive law appears almost unaffected by the layer thickness. Moreover, temperature and strain rate influence the cohesive laws. In an experimental study (Carlberger et al. 2009), it is shown that the peak stress in peel loading decreases monotonically with increasing temperature from -40°C to $+80$°C; the glass transition temperature is about $+90$°C for this adhesive. It is also shown that the fracture energy is fairly unaffected by the temperature in this temperature range. Effects of strain rate are also studied through a span of five decades from 10^{-4} to $10^{1}\,\mathrm{s}^{-1}$. Both the fracture energy and the peak stress appear to increase logarithmically with increasing strain rate in peel loading. However, the influence on the fracture energy is weak. The fundamental difference in influences of temperature, strain rate and thickness on the peak stress and fracture energy suggests different mechanisms as responsible for these properties of a cohesive law.

The peak stress and the yield strength of the adhesive also appear similar in size (Andersson and Stigh 2004). However, if we consider the constraint of the adhesive layer due to the large stiffness of the adherends, cf. the discussion in Sect. 2, the yield strength should be much larger in the constrained state than in a tensile test. That is, if we assume a state of deformation of the adhesive layer where the in-plane strains are zero and the strain in the peel direction is the same at all positions in the peel direction, ordinary plasticity theory leads to an increase of the yield strength with a factor of about three. This suggests that the mechanisms responsible for macroscopic yielding of the adhesive operate on a much smaller length scale than the layer thickness of the adhesive, in this case 0.2 mm. Moreover, with a newly developed experimental technique, it has been possible to deduce which model of in-elasticity, i.e. plasticity or damage, that gives the best correspondence with the macroscopic behaviour of the adhesive (Biel 2008). For the present adhesive, the experiments show no macroscopic plasticity. That is, on unloading from a severely deformed state, the adhesive behaves according to an elastic-damage cohesive model, cf.

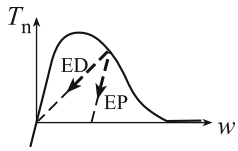

Fig. 11 Models for elastic-damage (ED) and elastic-plastic (EP) cohesive laws

Fig. 11. An interpretation of these observations is that inelasticity of epoxy in tensile loading is essentially due to a damage mechanism. In compressive loading, a damage mechanism is less plausible and inelasticity starts at a larger compressive load than in tension. It is noted that the conventional method to model this difference in "yield strength" in tension and compression is by use of a plasticity model dependent on the first stress invariant.

Though a number of experimental techniques are under development to measure cohesive properties, some of these properties are exceedingly hard to measure. This might be taken as an indication that they are unimportant; if they do not show themselves plainly in an experiment, they are probably not important. This is partly a correct conclusion. However, cohesive properties vary from specimen to specimen even if the experiments are performed with utmost care, cf. e.g. Andersson and Biel (2006). This means that conclusions regarding material properties should be deducible using one specimen and repeated experiments should be performed to learn about the variability in the property between different specimens. To support the development of cohesive laws and improve our understanding of the mechanics of thin adhesive layers, mesomechanical models have been developed (Salomonsson and Andersson 2008).

4 Mesomechanical modelling

The microscopic study discussed above indicates a complex mesomechanical process during fracture. To this end, a mesomechanical model is developed. This model acts as a representative volume element (RVE) of the adhesive layer. It is used to improve the understanding of the fracture process and to extrapolate experimental data (Salomonsson 2008; Salomonsson and Stigh 2009). The starting point in the development of the RVE is the geometry of the layer, cf. Fig. 2. An image processing method is used to identify mineral and epoxy regions. Based on this, a FE-mesh is designed, cf. Fig. 12. The mesh is large enough to be representative and detailed enough to capture the essential aspects of the fracture process. All conventional elements in the mesh are surrounded by cohesive elements to allow for a fracture process on the smaller length scale as shown in Figs. 4 and 5, cf. Xu and Needleman (1994). Using an evolution algorithm, the parameters of the constitutive models used for the matrix (epoxy), the particles (mineral) and the interfaces are determined to fit experimental data. By requiring good fit to cohesive laws in pure peel and pure shear loading, a unique set of parameters is determined (Salomonsson and Andersson 2008).

In Salomonsson (2008), the model is used to study mixed mode loading of the adhesive layer. It is shown how the mode mix influences the cohesive laws on the structural length scale. Moreover, the model shows how plasticity and decohesion influence the fracture process on the mesomechanical length scale. At pure peel loading, decohesion dominates and with an increasing shear component in the load mix, plasticity is more and more important. Thus, in pure shear, decohesion is accompanied by substantial plasticity leading to a much larger fracture energy in shear than in peel. It is also shown how compressive peel stress accompanies shear loading if the peel deformation is constrained, i.e. if $w = 0$. This explains the peel deformation observed in ENF-experiments (Leffler et al. 2007), and the shear hackles or cusps observed on fracture surfaces (Pettersson et al. 2006). Moreover, if it is assumed that the plasticity

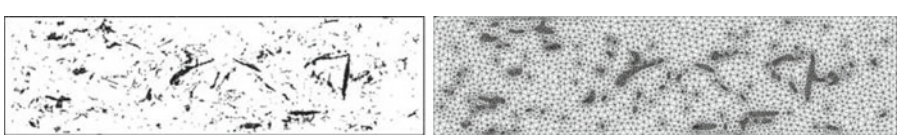

Fig. 12 Identification of material regions from a SEM-image. The *left* figure shows a SEM-image with enhanced contrast. The mineral regions are clearly identified as the dark areas. The *right* figure shows an unstructured FE-mesh with 7276 elements. The elements falling into the dark areas are given the properties of the mineral shown

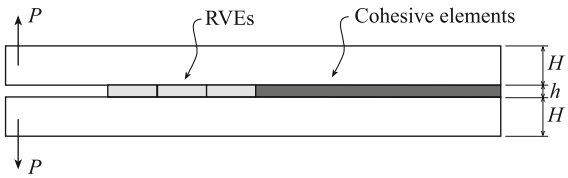

Fig. 13 Double cantilever beam specimen. *Light gray* zones indicate representative volume elements used in simulations, *dark gray* regions indicate cohesive elements. Not to scale

is time dependent in nature, it also explains the difference in influence of strain rate on cohesive laws in peel and shear; experiments indicate a much larger rate dependence on the peak stress in shear than in peel (Carlberger et al. 2009). With a smaller strain rate and a viscous type of plasticity, more time is available to decrease the stress resulting in a smaller peak stress. If this conjecture is accepted, it gives one more support for the idea that the two properties of cohesive laws: fracture energy and peak stress are determined by fundamentally different processes on the micromechanical length scale since the effect of strain rate on fracture energy is much smaller than on peak stress.

The mesomechanical model is also used to improve our understanding of the basic experimental methods developed to measure cohesive laws. In Salomonsson and Stigh (2009), the DCB-experiment is simulated using two different models of the adhesive: (1) a detailed model with a stacking of RVEs after each other, cf. Fig. 13 and (2) using the conventional cohesive elements COH2D4 available in Abaqus v. 6.5-1. The two models give the same behaviour when loaded in pure peel. When simulating the DCB-experiments using elastically deforming adherends and evaluating the simulations using the method described in Sect. 3, the two models give very similar cohesive laws and load vs. load point displacement curves. That is, in this case, conventional cohesive elements acting on the structural length scale are adequate to capture the behaviour. However, when allowing for large plastic deformation of the adherends, the results from the two models diverge. The detailed model shows more than 30% larger fracture energy than the model using cohesive elements. The reason is the large in-plane straining of the adhesive layer associated with the large plastic strains of the adherends. Experimentally, the same result is observed in Andersson and Biel (2006). Fortunately, the influence of in-plane straining can accurately

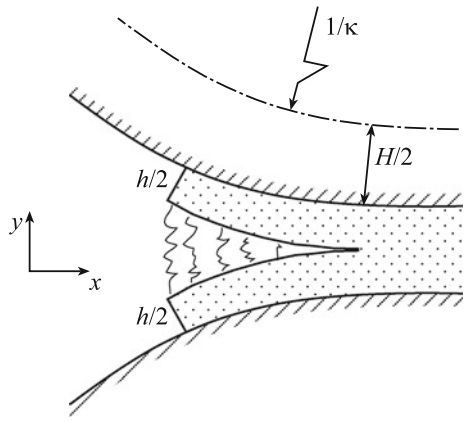

Fig. 14 Deformation of adhesive layer at a late stage of loading. At this moment, strain energy is trapped in the adhesive due to in-plane stretching of the *left* end of the adhesive. One dominant cohesive zone has been formed; indicated in the figure. The cohesive stress is at this moment minute since the crack is about to propagate

be captured if the in-plane straining is allowed to result in elastic in-plane stress, cf. Fig. 14.

A mesomechanical study also reveals the details of crack initiation in a DCB specimen (Salomonsson and Stigh 2009). Due to the constraints of the adherends, the micromechanical peel stress increases from the crack tip of the adhesive layer into the layer. That is, the first occurrence of the critical peel stress, on the micromechanical length scale, occurs several layer thicknesses into the adhesive layer. In other words, the first micro cracks appear somewhat into the adhesive layer and not at the crack tip. With less stiff adherends, this point moves closer to the crack tip, cf. Figs. 10 and 11 in Salomonsson and Stigh (2009).

5 Structural modelling and computational aspects

Modern product development is intimately linked to the possibility to perform and rely on simulations, i.e. finite element analyses. With complex structures, limited computational capacity and time, rational methods should be accurate enough but not unnecessarily detailed. An example is provided by crashworthiness analyses of cars and lorries. Here, the FE-models are designed to be accurate enough and still facilitate a run-time of less than about 17 h (Carlberger 2008). Typical joints in these structures are today performed using spot-welds and to a lesser degree by e.g. laser

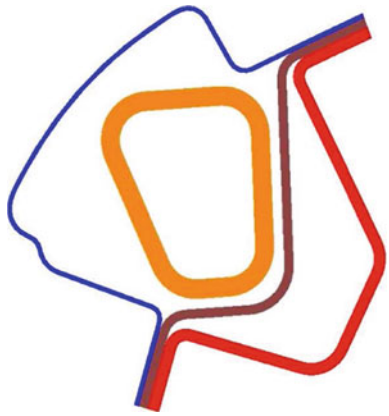

Fig. 15 Sketch of cross section of an A-pillar of a modern car. The pillar is built-up of four different shell structures. (Saab 9-3 cabriolet, currently joined with spot- and arc welds.)

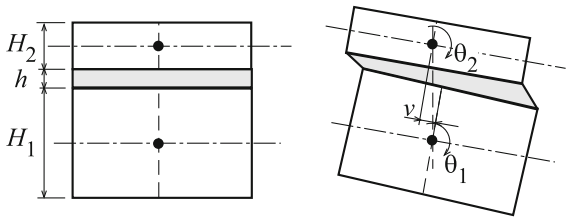

Fig. 16 Schematic of coupling of rotational degrees of freedom θ_1 and θ_2 of shell to shear deformation v of adhesive layer

welds and clinching. This limits the choice of materials that can be used in an automotive structure. By considering adhesives, the number of possible materials increases dramatically and reduction in weight is foreseen. A number of simulation related problems needs however to be mastered before a more frequent use will be seen. A typical joint is used to bond sheet metal of less than about one millimeter thickness. In a joint, two or more sheets can be bonded in parallel, cf. Fig. 15. These sheets are modelled as shells in FE-simulations. In shell elements, the degrees of freedom are the translations and rotations of the nodes, cf. e.g. Belytschko et al. (2000). The coupling of the rotational degrees of freedom to the deformation of the adhesive layer needs special consideration, cf. Carlberger et al. (2008), Salomonsson and Stigh (2009). Figure 16 shows a small deformation illustration of the coupling. In Carlberger et al. (2008), a small deformation formulation for an interphase element is derived. The coupling is considered in the kinematics and kinetics of the element. For instance, the shear deformation is given by $v = u_1 - u_2 + \theta_1 H_1/2 + \theta_2 H_2/2$, where u_α, θ_α, and H_α are the in-plane displacements, the clockwise rotations, and the thicknesses of the lower ($\alpha = 1$) and upper shell ($\alpha = 2$), respectively. A large deformation formulation is provided in Salomonsson and Stigh (2008). In this formulation, the simplified method to take account of the effects of in-plane straining discussed above is also included.

With explicit FE-analysis, the time-stepping algorithm is conditionally stable. This means that the time step must be chosen to be smaller than the critical time step, $\Delta t_c = 2/\omega_{max}$, where ω_{max} is the maximum eigenfrequency of the structure, cf. e.g. Belytschko et al. (2000). Straight forward calculation of the eigenfrequency necessitates the calculations of the mass and stiffness matrixes. This would destroy one of the principal advantages with explicit FE-analysis, namely that these memory demanding matrixes are not needed. To this end, the maximum eigenfrequency and critical time step are normally estimated using the Courant-Friedrichs-Lewy (CFL) estimate. This gives the critical time step as the time it takes an elastic wave with velocity c to pass between two nodes with the distance L, i.e. $\Delta t_c \geq L/c$. As cohesive elements are as thin as the adhesive layer, it is expected that cohesive elements would demand a very short time step in order to provide a stable numerical algorithm. Simulations with commercial FE-codes indicate that these programmes chose a time step according to the CFL-estimate. However, numerical experiments show that a substantially larger time step than given by the CFL-estimate is possible (Carlberger et al. 2008). In Stigh and Andersson (2010), an estimate of the critical time step of cohesive elements is derived. In essence, it shows that some of the mass provided by the adherends connected to the cohesive element can be regarded as a property of the cohesive element. Thus, the influence of cohesive elements on the maximum eigenfrequency is often substantially smaller than expected if the cohesive element is considered isolated from the mesh. As expected, the effects of the mass of the adhesive is usually immaterial (Carlberger et al. 2008). A study of effects of time step on the behaviour of a structure with an elastic-damage model of a cohesive zone (Fig. 11) is given in Carlberger and Stigh (2007). By choosing a long, but numerically stable time step, fracture is predicted by the simulation even when a shorter time step results in a dormant fracture process. That is, cohesive models using the elastic-damage model and long time steps appears to be conservative in a design process.

Numerical experiments show that a small number of cohesive elements suffice to span the process zone in order to achieve reasonable numerical accuracy, cf. Carlberger (2008). In designing the FE-mesh, simple formulas to estimate the length, d, of a fully developed process zone are therefore needed. For slender, beam-like bodies loaded in pure peel or pure shear, estimates are provided by

$$d_{\mathrm{est,peel}} = \sqrt{w_{\mathrm{c}}}\sqrt[4]{\frac{EH^3}{12J_{\mathrm{c,peel}}}}, \tag{7}$$

$$d_{\mathrm{est,shear}} = v_{\mathrm{c}}\sqrt{\frac{EH}{12J_{\mathrm{c,shear}}}} \tag{8}$$

Here, w_{c} and v_{c} are the critical peel and shear deformation of the cohesive laws in pure peel and shear loading, respectively; $J_{\mathrm{c,peel}}$ and $J_{\mathrm{c,shear}}$ are the areas under the cohesive laws in pure peel and shear loading, respectively; E and H are Young's modulus and the height of the adherends, respectively; both adherends are assumed identical and linearly elastic. As noted from the equations, d depends not only on the properties of the cohesive law but also on the stiffness of the adherends. The stiffer the adherends, the longer the process zone. Though these expressions are independent of the type of loading, i.e. bending moment, normal- or transversal forces, the type of loading also influences the size of the process zone, cf. Stigh (1988). This detail is not captured by the estimates. However, the difference in size of a fully developed process zone for differences in the applied loading is generally smaller than the influence of other properties not captured by the estimates. Tables 2 and 3 show comparisons between the estimated lengths and results from simulations. For guidance in the design of FE-meshes, the estimates appear accurate enough. Similar estimates are provided in e.g. Yang and Cox (2005); Turon et al. (2007). As noted from the tables, the length of the fully developed process zone is often larger than the height of the adherends. This supports the use of beam or shell theory to model the adherends, cf. e.g. Östlund and Nilsson (1993).

As noted above in Sect. 3, some test specimens are not very sensitive to the details of the cohesive law. One reason for this is that the size of the process zone is short compared to other relevant length scales. That is, a situation equivalent to the condition for small scale yielding (SSY) in fracture mechanics. If this is the case, the demands of a dense FE-mesh can be eased, cf. Turon et al. (2007). As long as SSY holds, the details of the cohesive law is immaterial for the structural behaviour as long as the the fracture energy is kept constant. Thus, we may vary the shape of the cohesive law to increase the length of the process zone and by this allowing a coarser FE-mesh as long as the conditions for SSY holds.

Table 2 Comparison of estimated length of the fully developed process zone and the length calculated from FE-simulation. Pure peel deformation from loading in DCB specimens, Andersson and Biel (2006)

H (mm)	4.5	10.6	16.6	20.7
d (mm)	7	14	18	23
$d_{\mathrm{est,peel}}$ (mm)	8.6	16.4	23	27

Table 3 Comparison of estimated length of the fully developed process zone and the length calculated from FE-simulation. Almost pure shear deformation from loading in ENF-specimens, Leffler et al. (2007). Each experiment has been simulated separately which gives some variation in d

H (mm)	16	25	32
d (mm)	42–45	34–54	61–75
$d_{\mathrm{est,shear}}$ (mm)	53	66	75

6 Conclusions

Geometrically, a cohesive zone is a surface allowing a continuum to be separated into two crack surfaces. It is argued that the surface models the behaviour of a material volume. This means that cohesive laws reflect the homogenized properties of the material. Thus, cohesive laws should be considered as material properties and not mere computational models. Problems with a straight forward application of a homogenization process are discussed. Techniques to measure cohesive laws are presented. These methods are based on the assumption of the existence of a unique cohesive law. For adhesive layers, measured cohesive laws are reasonably independent of the properties of the bonded parts. Moreover, simulated structural behaviour shows good agreement with experimentally measured properties. These observations support the validity of the model.

Experiments and simulations show promising results for the usefulness of cohesive models of adhesive layers. A number of different test set-ups have been developed to measure cohesive laws. These methods are

based on the path independence of the J-integral. To date, a limited experience exists on the influence of important properties as temperature, loading rate and layer thickness on the cohesive properties of adhesives; only a very limited number of materials have been tested. Even less experience exists on effects of mixed mode loading.

Finite element formulations for structural analyses need correct coupling of the rotational degrees of freedom to the deformation of the adhesive layer.

Acknowledgments Former and present coworkers and students at the University of Skövde are acknowledge for fruitful discussions. Financial support from EU's 6th frame programme through FUTURA IP, and VINNOVA through the FFP-project Crashworthiness and the KSP-project Demo-lim are gratefully acknowledged.

References

Adams RD, Comyn J, Wake WC (1997) Structural adhesive joints in engineering. 2. Springer, Berlin

Alfredsson KS (2003) On the determination of constitutive properties of adhesive layers loaded in shear an inverse solution. Int J Fract 123:49–62

Alfredsson KS (2004) On the instantaneous energy release rate of the end-notch flexure adhesive joint specimen. Int J Solids Struct 41:4787–4807

Alfredsson KS, Stigh U (2009) Stability of beam-like fracture mechanics specimens (submitted)

Andersson T, Biel A (2006) On the effective constitutive properties of a thin adhesive layer loaded in peel. Int J Fract 141(1–2):227–246

Andersson T, Stigh U (2004) The stress-elongation relation for an adhesive layer loaded in peel using equilibrium of energetic forces. Int J Solids Struct 41:413–434

Bäcklund J (1981) Fracture analysis of notched composites. Comput Struct 13:145–154

Bao G, Suo Z (1992) Remarks on crack-bridging concepts. Appl Mech Rev 24:355–366

Barenblatt G (1962) The mathematical theory of equilibrium cracks in brittle fracture. Adv Appl Mech 7:55–129

Belytschko T, Liu WK, Moran B (2000) Nonlinear finite elements for continua and structures. Wiley, London

Biel A (2008) Mechanical behaviour of adhesive layers, F1-F18, Thesis for the degree of PhD, Chalmers University of Technology, Göteborg

Carlberger T (2008) Adhesive Joining for Crashworthiness, D1-D11, Thesis for the degree of PhD, Chalmers University of Technology, Göteborg

Carlberger T, Stigh U (2007) An explicit FE-model of impact fracture in an adhesive joint. Eng Fract Mech 74:2247–2262

Carlberger T, Alfredsson KS, Stigh U (2008) FE-formulation of interphase elements for adhesive joints. Int J Comput Methods Eng Sci Mech 9(5):288–299

Carlberger T, Biel A, Stigh U (2009) Influence of temperature and strain rate on cohesive properties of a structural epoxy adhesive. Int J Fract 155:155–166

Chai H (1986) Bond thickness effect in adhesive joints and its significance for mode I interlaminar fracture of composites. In: Composite materials: testing and design, ASTM STP 893, Philadelphia, pp 209–231

Cox BN, Yang QD (2007) Cohesive zone models of localization and fracture in bone. Eng Fract Mech 74:1079–1092

Dávila CG, Rose CA, Camanho PP (2009) A procedure for superposing linear cohesive laws to represent multiple damage mechanisms in the fracture of composites. Int J Fract 158:211–223

Goland M, Reissner E (1944) The stresses in cemented joints. ASME J Appl Mech 66:A17–A27

Groth H (1988) Stress singularities and fracture at interface corners in bonded joints. Int J Adh Adhesives 8(2):107–113

Hillerborg A, Modéer M, Petersson P-E (1976) Analysis of crack formation and crack growth in concrete by means of fracture mechanics and finite elements. Cement Concrete Res 6:773–782

Högberg JL, Sørensen BF, Stigh U (2007) Constitutive behaviour of mixed mode loaded adhesive layer. Int J Solids Struct 44:8335–8354

Kinloch AJ (1987) Adhesion and adhesives—science and technology. Chapman and Hall, London

Leffler K, Alfredsson KS, Stigh U (2007) Shear behaviour of adhesive layers. Int J Solids Struct 44:530–545

Needleman A (1987) A continuum model for void nucleation by inclusion debonding. ASME J Appl Mech 54:525–531

Nilsson F (2001) Fracture mechanics—from theory to applications. Department of Solid Mechanics, KTH, Stockholm

Nilsson F (2006) Large displacement aspects on fracture testing with double cantilever beam specimen. Int J Fract 139:305–311

Olsson P, Stigh U (1989) On the determination of the constitutive properties of thin interphase layers An exact inverse solution. Int J Fract 41(4):R71–R76

Östlund S, Nilsson F (1993) Cohesive zone modelling of damage at the tip of cracks in slender beam structures. Fatigue Eng Mater Struct 16(6):663–676

Paris AJ, Paris PC (1988) Instantaneous evaluation of J and C^*. Int J Fract 38:R19–R21

Pettersson KB, Neumeister JM, Gamstedt K, Oberg H (2006) Stiffness reduction, creep, and irreversible strains in fiber composites tested in repeated interlaminar shear. Compos Struct 76(1–2):151–161

Rice JR (1968) A path independent integral and the approximative analysis of strain concentration by notches and cracks. ASME J Appl Mech 88:379–386

Salomonsson K (2008) Mixed mode modeling of a thin adhesive layer using a meso-mechanical model. Mech Mater 40(8):665–672

Salomonsson K, Andersson T (2008) Modeling and parameter calibration of an adhesive layer at the meso level. Mech Mater 40(1–2):48–65

Salomonsson K, Stigh U (2008) An adhesive interphase element for structural analyses. Int J Numer Meth Eng 76:482–500

Salomonsson K, Stigh U (2009) Influence of root curvature on the fracture energy of adhesive layers. Eng Fract Mech 76(13):2025–2038

Schmidt P (2008) Modelling of adhesively bonded joints by an asymptotic method. Int J Eng Sci 46:1291–1324

Sørensen BF, Jacobsen TK (1998) Large-scale bridging in composites: R-curves and bridging laws. Compos Part A 29: 1443–1451

Sørensen BF, Kirkegaard P (2006) Determination of mixed mode cohesive laws. Eng Fract Mech 73:2642–2661

Stigh U (1987) Initiation and growth of an interface crack. In: Mechanical behaviour of adhesive joints, Bordeaux, France: Pluralis, Paris, France

Stigh U (1988) Damage and crack growth analysis of the double cantilever beam specimen. Int J Fract 37:R13–18

Stigh U, Andersson T (2010) Critical time step for cohesive elements and explicit FEA, (submitted)

Stigh U, Alfredsson KS, Biel A (2009) Measurement of cohesive laws and related problems. In: Proceedings of ASME international mechanical engineering congress and exposition Lake Buena Vista, Florida, USA

Sun C, Thouless MD, Waas AM, Schroeder JA, Zavattieri PD (2008) Ductile-brittle transitions in the fracture of plastically-deforming, adhesively-bonded structures: II numerical studies. Int J Solids Struct 45:4725–4738

Turon A, Dávila CG, Camanho PP, Costa J (2007) An engineering solution for mesh size effects in the simulation of delamination using cohesive zone models. Eng Fract Mech 74:1665–1682

Tvergaard V, Hutchinson JW (1992) The relation between crack growth resistance and fracture process parameters in elastic-plastic solids. J Mech Phys Solids 40:1377–1397

Xu XP, Needleman A (1994) Numerical simulations of fast crack growth in brittle solids. J Mech Phys Solids 42:1397–1434

Yang Q, Cox B (2005) Cohesive models for damage evolution in laminated composites. Int J Fract 133:107–137

Yang QD, Thouless MD (2001) Mixed-mode fracture analyses of plastically-deforming adhesive joints. Int J Fract 110:175–187

Yang QD, Cox BN, Nalla RK, Ritchie RO (2006) Re-evaluating the toughness of human cortical bone. Bone 38:878–887